applied sciences

MDPI

Article

Research on the Whirling and Vibration Characteristics of Steel–Titanium Alloy Composite Drill Strings for Ultra-Deep Wells

Jianjun Wang [1,*], Siqi Yang [1], Xuejun Hou [2,3,*], Hongfei Luo [3,2], Weihuang Hou [2], Shen Hao [2], Menghan Yan [2], Yongkang Wang [2], Anqing Fu [1], Tiancheng Huang [4] and Qiao Deng [5]

1 State Key Laboratory of Oil and Gas Equipment, CNPC Tubular Goods Research Institute, Xi'an 710077, China; yangsiqi@cnpc.com.cn (S.Y.); f2378947910@126.com (A.F.)
2 College of Petrol Engineering, Chongqing University of Science and Technology, Chongqing 401331, China; shenhaofox_0412@foxmail.com (S.H.); decymh@outlook.com (M.Y.); wangyong.kang@foxmail.com (Y.W.)
3 School of Mechanical Engineering, Xinjiang University, Urumqi 830017, China; luohongfei193@foxmail.com
4 School of Mechanical Engineering, Yangtze University, Jingzhou 434023, China; huangtch@yangtzeu.edu.cn
5 School of Petroleum Engineering, Yangtze University, Wuhan 430100, China; dengqiao@yangtzeu.edu.cn
* Correspondence: wangjianjun005@cnpc.com.cn (J.W.); xuejun_hou_2013@163.com (X.H.)

Abstract

To address whirling- and vibration-induced failures in ultra-deep well drill strings caused by high slenderness ratios and complex loading conditions, this study establishes a nonlinear dynamic finite element model for a steel–titanium alloy composite drill string. The model is discretized with Euler–Bernoulli beam elements and solved using Newmark time integration combined with an iterative node-based spatial solution. Weight on bit, torque, wellbore–wall friction, impact/contact force, and equivalent drilling-fluid damping are considered. The model is used to evaluate how titanium alloy section size, length, wall thickness, and installation position affect whirling, lateral vibration, and torsional vibration. The results show that increasing drill-string diameter reduces the whirling range and lateral vibration intensity; when the diameter exceeds 149.23 mm, wall-impact frequency decreases markedly. Although the titanium alloy section exhibits approximately 60% higher local lateral vibration intensity than the steel section, the upper steel section experiences an approximately 18% reduction in lateral vibration. Installing the titanium alloy section in the middle of the string rather than near the bit reduces the overall lateral vibration intensity by approximately 30% and torsional vibration intensity by approximately 40%. Based on comparative sensitivity analysis, a titanium alloy section length of 1000–2000 m, diameter not less than 139.7 mm, and wall thickness not less than 12.7 mm are recommended for the simulated ultra-deep well conditions. These findings provide quantitative guidance for safer and more stable composite drill-string design.

Keywords: ultra-deep wells; steel–titanium alloy drill string; vibration characteristics; whirling characteristics; nonlinear dynamics

Academic Editor: Ján Dižo

Received: 25 May 2026
Revised: 24 July 2026
Accepted: 3 August 2026
Published: 14 September 2026

1. Introduction

As the drilling depths in ultra-deep and extra-deep wells continue to increase, drill strings are subjected to increasingly severe combined loads, including tension, bending, torsion, and vibration, which raises the risk of failure [1,2]. Titanium alloys have low density, high specific strength, and excellent corrosion and fatigue resistance, making them promising materials for reducing drill-string self-weight, lowering friction, and extending drilling reach. However, combining titanium alloy drill pipes with conventional steel drill pipes introduces substantial differences in the elastic modulus, density, and other material properties. These differences can change the stiffness distribution and mass configuration of the full drill-string system and may produce distinctive dynamic behavior. Therefore, a systematic investigation of the whirling and vibration characteristics of steel–titanium alloy composite drill strings is essential for the safe and efficient application of this technology in ultra-deep wells.

Research on drill-string dynamics has advanced from early summaries of vibration types and mechanisms [1,2] to theoretical modeling and analyses of nonlinear coupled vibrations, including stick–slip and whirling motion [3–6]. Experimental studies and field measurements have improved the understanding of complex drill-string motion through model tests [7,8] and downhole measurements [9,10]. With the increasing challenges of ultra-deep wells, recent work has focused on full-depth dynamic simulations [11,12] and coupled vibration analyses under extreme operating conditions [13,14]. Studies have also clarified the effects of drill-string whirling and related safety thresholds. For example, finite element contact models have been used to evaluate casing wear caused by drill-string whirling and to emphasize the need to avoid critical rotational speeds [15]. Three-dimensional dynamic models that include compression, torque, and rotation have also been developed to investigate buckling and friction transmission [16]. In addition, numerical simulations have shown that, under ultra-deep well conditions exceeding 9000 m, the coupling of whirling and stick–slip vibration near the neutral point is particularly strong and poses significant safety risks [17,18].

Recent studies have also emphasized torsional-axial coupling, stick–slip instability, and dynamic failure in rotary drilling systems. Kessai et al. analyzed tool-string dynamic failure and lifetime under coupled torsional-axial vibration [19] and further investigated drill-bit deformation under large-amplitude stick–slip vibration [20]. These studies show that torsional stiffness variation, bit deformation, and coupled vibration may strongly influence drilling stability and fatigue failure. They provide an important basis for discussing the possible stick–slip implications and limitations of the present steel–titanium alloy composite drill-string model.

From the perspective of numerical methodology, eigensensitivity analysis and model-order reduction for damped rotating systems also provide useful references for improving large-scale finite element dynamic models and Campbell-type response analyses [21,22]. In addition, reducing the vibration, wear, and premature drill-string failure can improve the resource efficiency and operational safety, which is consistent with the sustainable infrastructure and responsible production objectives emphasized in the United Nations Sustainable Development Goals, especially SDGs 9, 12, and 13 [23].

Our previous work systematically examined the influence of drilling parameters, such as the rotational speed, weight on bit, and mud density, on the whirling and vibration characteristics of all-steel drill strings in ultra-deep wells. However, that work mainly focused on optimizing the operating parameters for homogeneous all-steel drill strings. When titanium alloy is introduced to form a composite drill string, the dominant factors governing the dynamic response shift from the operating parameters to the structural design parameters. In recent years, increasing attention has been paid to improving drill-string dynamic performance through material selection and structural optimization. Cheng Jinhua [24] studied the whirling characteristics and joint strength of aluminum–alloy drill pipes, whereas Liu Qiang, Chen Feng, and co-workers [25,26] proposed a titanium alloy/steel composite drill-string design and preliminarily demonstrated its potential for reducing dynamic stress. Nevertheless, clear design criteria and comprehensive theoretical explanations are still lacking for how the size, installation position, length, and wall thickness of the titanium alloy section affect the overall whirling and vibration responses of composite drill strings.

The novelty of this work is that it focuses on the structural-parameter sensitivity of a long steel–titanium alloy composite drill string under ultra-deep well conditions, rather than only on operating-parameter optimization or general titanium/steel composite concepts. Specifically, the study jointly evaluates the titanium alloy section size, length, wall thickness, and installation position within the same nonlinear dynamic framework and links these parameters to the whirling range, wall-impact tendency, lateral vibration, and torsional vibration. The results are intended to support a structural design framework and parameter-matching strategy for titanium alloy–steel composite drill strings, thereby improving the safety, reliability, and drilling capacity of ultra-deep well drill-string systems.

2. Materials and Methods

This section describes the composite drill-string configuration, material parameters, loading scenarios, dynamic model, boundary conditions, contact model, and numerical solution procedure. The finite element equations were solved using the authors' numerical implementation based on Euler–Bernoulli beam elements, Newmark time integration, and node-by-node spatial iteration.

2.1. Composite Drill-String Configuration and Structural Parameters

As shown in Figure 1, ultra-deep well drilling exposes the drill string to complex loads, including tension, compression, bending, and torsion. For steel–titanium alloy composite drill strings, the dynamic behavior is governed not only by these external loads but also by the heterogeneous material properties and structural configuration of the composite system.

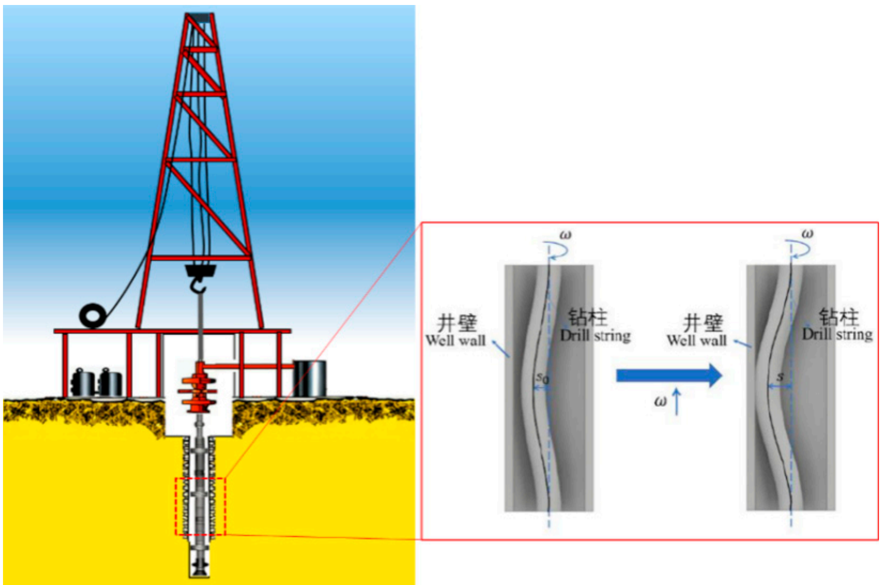

Figure 1. Schematic diagram of drilling.

Previous studies have shown that the whirling and vibration responses of all-steel drill strings are mainly controlled by drilling parameters such as the rotational speed and weight on bit [18]. In contrast, when steel and titanium alloy are combined in the same drill string, the structural configuration of the titanium alloy section becomes a key factor controlling the stiffness distribution, mass distribution, and dynamic response of the system. Accordingly, this study investigates the mechanisms by which the following structural design parameters affect the dynamic characteristics of the composite drill string:

(1) The size of the titanium alloy drill-string section directly affects its bending stiffness and moment of inertia.

(2) The installation position of the titanium alloy section determines the stiffness distribution and center of mass of the composite drill string, thereby affecting its dynamic stability.

(3) The length of the titanium alloy section controls the proportion and effective range of the lightweight section within the overall drill string.

(4) Together with the section diameter, the wall thickness of the titanium alloy section determines the bending and torsional moments of inertia of the cross section.

Clarifying the effects of these structural parameters on whirling and vibration is necessary for developing a sensitivity-analysis-based composite drill-string design. Such a design must balance weight reduction and dynamic stability to ensure safe ultra-deep well drilling.

2.2. Geometric and Physical Parameters of the Drill String

Using the established nonlinear dynamic finite element model for an ultra-deep well drill string, this study evaluates the dynamic characteristics of a composite drill string at a well depth of 15,000 m. The analysis focuses on key structural parameters, including the dimensions, installation positions, and lengths of the titanium alloy drill-string section. The drill-string combination schemes are listed in Table 1, and the basic calculation conditions are summarized in Table 2.

Table 1. Drilling collar combination schemes.

Plan	Drill String Assembly	Factor
1	139.7 mm × 12.7 mm, 165 ksi steel drill pipe + 139.7 mm × 12.7 mm, 135 ksi titanium alloy drill pipe, 1000 m drill string with bottom-hole assembly (BHA).	Drill string size
2	149.23 mm × 14.5 mm, 165 ksi steel drill pipe + 149.23 mm × 14.5 mm, 135 ksi titanium alloy drill pipe, 1000 m drill string with bottom-hole assembly (BHA).	
3	168.28 mm × 15.88 mm, 165 ksi steel drill pipe + 168.28 mm × 15.88 mm, 135 ksi titanium alloy drill pipe, 1000 m drill string with bottom-hole assembly (BHA).	
4	149.23 mm × 14.5 mm, 165 ksi steel drill pipe + 149.23 mm × 14.5 mm, 135 ksi titanium alloy drill pipe, 1000 m drill string with bottom-hole assembly (BHA).	Drill string installation location
5	149.23 mm × 14.5 mm, 165 ksi steel drill pipe + 149.23 mm × 14.5 mm, 135 ksi titanium alloy drill pipe, 1000 m + 149.23 mm × 14.5 mm steel drill pipe + BHA	
6	Φ149.23 × 15.88 mm, U165 steel drill pipe (upper section) + 139.7 × 10.54 mm, S135 steel drill pipe (bottom section, 0 m) + BHA	Titanium alloy drill string length
7	Φ149.23 × 15.88 mm, U165 steel drill pipe (upper section) + 139.7 × 10.54 mm, S135 steel drill pipe (bottom section, 1000 m) + BHA	
8	Φ149.23 × 15.88 mm, U165 steel drill pipe (upper section) + 139.7 × 10.54 mm, S135 steel drill pipe (bottom section, 2000 m) + BHA	
9	Φ149.23 × 15.88 mm, U165 steel drill pipe (upper section) + 139.7 × 10.54 mm, S135 steel drill pipe (bottom section, 3000 m) + BHA	

https://doi.org/10.3390/app16189097

Table 2. Calculation conditions.

Drill String Whirl—Calculation Conditions	
Titanium alloy drill string material	Elastic modulus: 120 GPa; Density: 4500 kg/m^3; Poisson's ratio: 0.3
Steel drill string material	Elastic modulus: 210 GPa; Density: 7800 kg/m^3; Poisson's ratio: 0.3
Drill collar eccentricity	0.001 m
Turntable speed	100 r/min
Weight on bit	50 kN
Mud density	1.2 g/cm^3
Friction coefficient	0.3
Wellbore parameters	Depth: 15,000 m; Diameter: 315 mm

2.3. Dynamic Model of the Composite Drill String

2.3.1. Basic Assumptions of the Model

To investigate how the structural parameters of the steel–titanium alloy composite drill string influence its dynamic response, the following assumptions are adopted when establishing the nonlinear dynamic model:

(1) The wellbore trajectory is assumed to be an ideal vertical well with a circular cross section.

(2) The influence of drill-string joints, which have a relatively small effect on the overall whirling characteristics, is neglected.

(3) Drill-string deformation is assumed to be small.

(4) Transverse shear strain is neglected.

(5) The stabilizer is represented as an equivalent drill-string section with a larger cross section.

(6) The drill string is discretized into three-dimensional elastic beam elements, with separate material parameters, including the elastic modulus and density, assigned to steel and titanium alloy elements.

(7) The direct effect of the drilling-fluid flow on the drill-string motion is ignored.

The above assumptions define the applicability of the model. The model is most suitable for near-vertical ultra-deep wells in which the overall whirling and vibration trends are dominated by drill-string structural parameters. For highly deviated or curved well trajectories, large deformation, local joint effects, and nonlinear fluid–structure interaction may alter the absolute vibration amplitude and local contact force. In the present model, drilling-fluid effects are represented mainly through equivalent damping in the Rayleigh damping matrix rather than through fully coupled fluid–structure interaction. Therefore, the results should be interpreted as comparative design trends among the tested schemes, while detailed prediction for specific field wells requires further calibration with downhole measurements or coupled fluid–solid simulations.

2.3.2. Dynamic Control Equations

For the steel–titanium alloy composite drill-string system, the spatial discretization is formulated using Euler–Bernoulli beam theory. The dynamic behavior of the composite system is governed by the following equation:

$$M\ddot{U} + C\dot{U} + KU = F \tag{1}$$

The global mass matrix M and stiffness matrix K are assembled from the material properties of the steel and titanium alloy sections (Table 2):

$$M = M_1 + M_2 \tag{2}$$

$$K = K_1 + K_2 \tag{3}$$

$$K_n = K_{n1} + K_{n2} + K_{n3} \tag{4}$$

where M is the system mass matrix, C is the damping matrix, K is the stiffness matrix, F is the external-force vector, and U, $\dot{U}$, and $\ddot{U}$ are the nodal displacement, velocity, and acceleration vectors, respectively. M_2 is the inertial mass matrix associated with rotation about the y and z axes. K_1 is the linear stiffness matrix, and K_n is the nonlinear stiffness matrix, which consists of three components: axial-force and bending-moment coupling (Kn_1), axial-force and torque coupling (Kn_2), and torque and bending-moment coupling (Kn_3).

The system damping matrix C is formulated in the Rayleigh damping form:

$$C = \alpha_r M + \beta_r K \tag{5}$$

where α_r and β_r are the Rayleigh damping coefficients, which are determined from the natural frequency of the system and the corresponding damping ratio. These coefficients represent the equivalent damping effect of the drilling fluid.

2.3.3. Boundary Conditions, Loads, and Contact Model

In the dynamic model, the boundary conditions of the drill-string system are defined as follows. At the wellhead, the lateral displacement of the drill string is constrained by a hinged support, while the string is driven by turntable torque. In the axial direction, a spring element is used to represent the elastic support provided by the surface equipment. At the bit end, the lateral displacement is constrained, and the bit is subjected to frictional torque from the formation. The axial direction at the bit is free, and the interaction between the bit and rock is simulated by applying the weight on bit. This dynamic bit–rock contact provides the axial and torsional excitation for the system.

(1) Weight on bit conditions and torque excitation

The weight-on-bit $W_b(t)$ fluctuates over time:

$$w_b(t). = w_{bd} + K_f dsin(2\pi n_b f_b t) \tag{6}$$

where w_{bd} is the average weight on bit (N), K_f is the formation stiffness (N/m), d is the cutting depth per bit revolution (m), n_b is the number of blades or cones, and f_b is the frequency of weight-on-bit fluctuation (Hz).

The frictional torque acting on the drill bit $T_b(t)$ can be expressed as

$$T_b(t) = \frac{1}{3} r_h \mu_f W_b(t) = \frac{1}{3} r_h \mu_f [W_{bd} + K_f dsin(2\pi n_b f_b t)] \tag{7}$$

where r_h is the borehole radius (m), and μ_f is the dynamic friction coefficient between the drill bit and the well wall.

(2) Collision model between drill string and well wall

A clearance-based contact criterion is adopted. As shown in Figure 2, collision is assumed to occur when the lateral displacement rio of the drill-string element centroid exceeds the annular clearance ($r_{io} \geq r_h - r_i$), and the contact force is calculated using Hertz contact theory. The radial contact force F_r, tangential friction force F_{tan}, and frictional resistance moment T_f are expressed as follows:

$$F_r = \begin{cases} -K_h(r_{io} + r_i - r_h)\ r_{io} \geq r_h - r_i \\ 0\ r_{io} \leq r_h - r_i \end{cases} \tag{8}$$

$$F_{tan} = -\mu_h F_r sgn\Omega \tag{9}$$

$$T_f = Ftanr_i \tag{10}$$

where K_h is the borehole-wall stiffness (N/m), r_{io} is the lateral displacement of the drill-string centroid (m), r_i is the outer radius of the drill string (m), μ_h is the dynamic friction coefficient between the drill string and the borehole wall, and Ω is the rotational speed of the drill string relative to the borehole wall (rad/s).

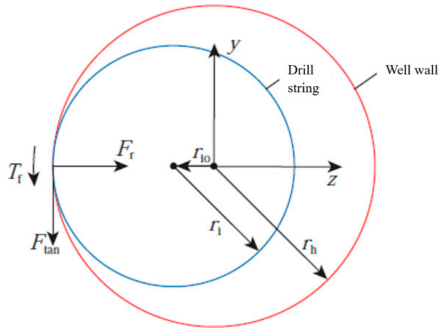

Figure 2. Collision model.

2.4. Numerical Solution Method

2.4.1. Time-Domain Discretization

The Newmark method is a widely used time-integration algorithm in structural dynamics and is applied here for time-domain discretization. It transforms the second-order differential equation of motion, expressed in terms of displacement, into a linear algebraic equation that can be solved directly at discrete time nodes.

The motion control equation of the drill string at any time t is

$$M\ddot{U}_t + C\dot{U}_t + KU_t = F_t \tag{11}$$

In the Newmark method, the velocity and displacement at time $t + \Delta t$ are approximated as follows:

$$\dot{U}_{t+\Delta t} = \dot{U}_t + [(1-\alpha)\ddot{U}_t + \alpha\ddot{U}_{t+\Delta t}]\Delta t \tag{12}$$

$$U_{t+\Delta t} = U_t + \dot{U}_t\Delta t + \left[(\frac{1}{2} - \beta)\ddot{U}_t + \beta\ddot{U}_{t+\Delta t}\right]\Delta t^2 \tag{13}$$

where α and β are weighting parameters.

Combining Equations (12) and (13) gives

$$\ddot{U}_{t+\Delta t} = \frac{1}{\beta\Delta t^2}(U_{t+\Delta t} - U_t) - \frac{1}{\beta\Delta t}\dot{U}_t - \left(\frac{1}{2\beta} - 1\right)\ddot{U}_t \tag{14}$$

$$\dot{U}_{t+\Delta t} = \frac{\alpha}{\beta\Delta t}(U_{t+\Delta t} - U_t) - \left(\frac{\alpha}{\beta} - 1\right)\dot{U}_t - \left(\frac{1}{2\beta} - 1\right)\ddot{U}_t\Delta t \tag{15}$$

Substituting Equations (14) and (15) into Equation (11) and rearranging gives

$$\begin{aligned}(\lambda_1 M + \lambda_4 C + K)U_{t+\Delta t} &= F_{t+\Delta t} + M(\lambda_1 U_t + \lambda_2 \dot{U}_t + \lambda_3 \ddot{U}_t) \\ &+ C(\lambda_4 U_t + \lambda_5 \dot{U}_t + \lambda_6 \ddot{U}_t)\end{aligned} \tag{16}$$

where $\lambda_1 = 1/(\beta\Delta t^2)$, $\lambda_2 = 1/(\beta\Delta t)$, $\lambda_3 = 1/(2\beta) - 1$, $\lambda_4 = \alpha/(\beta\Delta t)$, $\lambda_5 = \alpha/\beta - 1$, and $\lambda_6 = (\alpha/(2\beta) - 1)\Delta t$.

Using the displacement, velocity, acceleration, and external force at time t, the displacement at time $t + \Delta t$ can be obtained from Equation (16). The velocity and acceleration at time $t + \Delta t$ are then calculated from Equations (14) and (15). Therefore, the motion state at any time can be derived from the initial configuration.

2.4.2. Spatial Discretization

After time-domain discretization with the Newmark method, the displacement response at each time step is obtained using the node iteration method. The spatial solution strategy is shown schematically in Figure 3. In this method, three nodes and two elements are used as the basic calculation module, and the overall spatial configuration of the drill string is obtained through successive recursion based on local mechanical equilibrium.

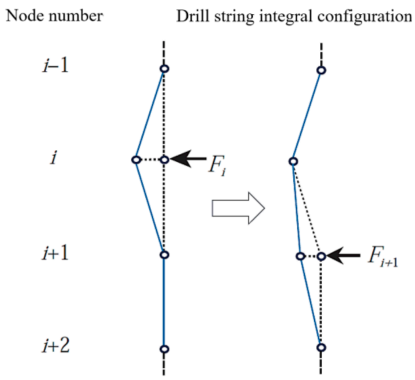

Figure 3. Schematic diagram of the node iteration method.

In the node iteration method, two elements and three nodes form the minimum computational unit. The displacements of nodes i and j are assumed to be known. Based on local mechanical equilibrium, the displacement of node k is calculated. The displacement of node l is then obtained from the displacements of nodes k and j, and the process is continued along the string. The equilibrium equation for node k can be written as follows:

$$F_i = [K_{i,i-1} \quad K_{i,i} \quad K_{i,i+1}][U_{i-1} \quad U_i \quad U_{i+1}]^T \tag{17}$$

The displacement of node i is

$$U_i = K_{i,i}^{-1}[F - (K_{i,i-1}U_{i-1} + K_{i,i+1}U_{i+1})] \tag{18}$$

After the nodal displacement is obtained, contact with the wellbore wall is evaluated immediately. Contact is assumed when the lateral displacement of the drill-string center exceeds the annular clearance. Once contact occurs, the Hertz contact model [27] is used to calculate the corresponding radial contact force and tangential friction force. The resulting nodal force and moment are added to the external-force vector, thereby enforcing the displacement constraint and preventing the drill string from penetrating the wellbore wall.

The solution starts from the top node of the drill string and proceeds sequentially to the bottom node. The calculation is then performed in the reverse direction from the bottom node to the top node using the latest displacement values. This procedure constitutes one iteration step. After several iterations, if the difference between the displacement results from two adjacent iterations is smaller than the prescribed tolerance, the solution is considered converged, and a stable spatial configuration of the drill string is obtained for that time step.

3. Results

3.1. Effect of Titanium Alloy Section Size on Composite Drill-String Dynamics

Figure 4 shows the whirling trajectories for drill-string combination schemes 1, 2, and 3 at different well depths. The intermittent and random collision force between the drill bit and the wellbore wall, together with torque fluctuations caused by the changing contact state between the bit and the bottomhole formation, produces irregular whirling near the bottom of the well. As well depth decreases, the whirling range of the drill string tends to increase. Near the wellhead, however, the whirling range is strongly restricted by the wellhead constraint. A larger titanium alloy drill-string section increases the stiffness and improves the resistance to lateral vibration. At the same time, damping from the drill-string structure and drilling fluid increases, reducing the collision intensity between the drill string and the wellbore wall. Consequently, the whirling velocity and whirling range decrease as the drill-string size increases. When the drill-string diameter exceeds 149.23 mm, the collision frequency between the drill string and wellbore wall decreases markedly, which helps reduce the vibration intensity and wear. These results are important for optimizing drill-string design and drilling conditions.

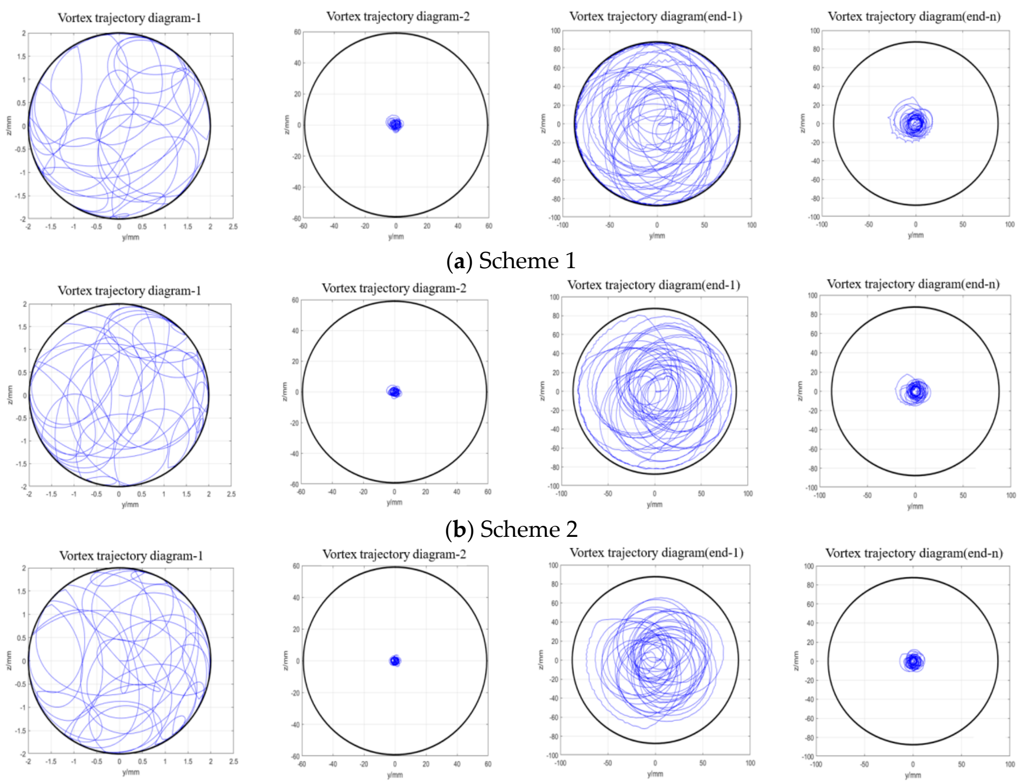

(**a**) Scheme 1

(**b**) Scheme 2

(**c**) Scheme 3

Figure 4. Whirling trajectory of drill bit, well depth 11,250 m, well depth 7500 m and well depth 250 m.

Figure 5 shows the whirling velocity of the drill string for combination schemes 1–3 at a well depth of 11,250 m. As the diameter of the titanium alloy drill string increases, its moment of inertia increases significantly. The coupling between the moment of inertia and the added mass increases the sensitivity of the dynamic response. In addition, the higher stiffness of the drill string reduces the energy dissipation through elastic deformation, allowing more input energy to be converted into a whirling motion. Therefore, the whirling velocity increases with the drill-string size.

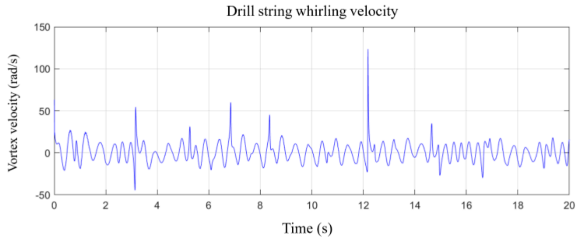

(**a**) Scheme 1

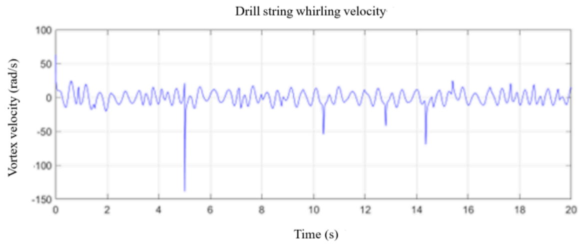

(**b**) Scheme 2

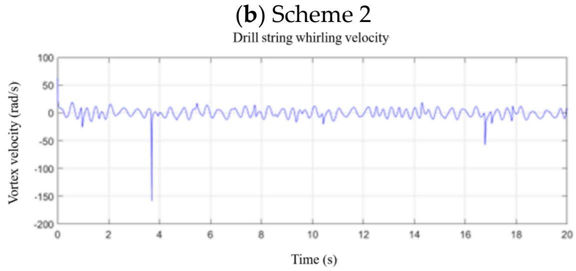

(**c**) Scheme 3

Figure 5. Whirling velocity of drill string at a depth of 11,250 m.

Figure 6 shows the lateral vibration of the drill string for combination schemes 1–3 as a function of the well depth. Increasing the drill-string diameter increases the system stiffness, improves the resistance to lateral deformation, and reduces the lateral vibration. Larger-diameter drill strings also experience stronger viscous damping from the drilling fluid, which further reduces the lateral vibration intensity. When the drill-string diameter exceeds 149.23 mm, the stiffness is sufficiently high that further increases provide limited additional benefit, and the lateral vibration intensity tends to stabilize. By contrast, the bending stiffness of the titanium alloy drill string is approximately 50% of that of the steel drill string, resulting in lower resistance to lateral loading. Under the same excitations, such as bit friction and wellbore collision, the titanium alloy string therefore undergoes higher bending deformation and exhibits higher lateral vibration intensity.

Figure 7 compares the lateral vibration curves of the composite drill string and the all-steel drill string. Unlike the all-steel string, the composite string changes the system stiffness distribution through a lower titanium alloy section and an upper steel section. This configuration reduces the suspended load carried by the upper steel drill string and weakens the inertial driving force associated with its lateral vibration. Because the titanium alloy section has lower stiffness, it becomes the main region for vibration-energy absorption and therefore shows increased vibration. The upper steel section benefits from its higher stiffness and from the buffering effect of the titanium alloy section, leading to reduced vibration levels. This behavior, in which the lower titanium alloy section absorbs vibration while the upper steel section experiences vibration mitigation, provides a theoretical basis for optimizing drill strings under deep-well and complex-wellbore conditions.

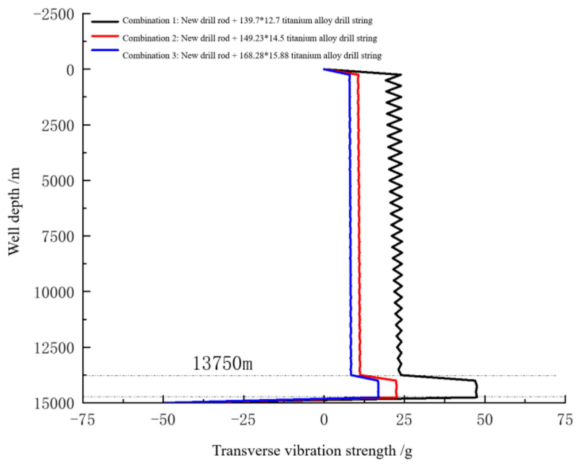

Figure 6. Transverse vibration strength of drill string.

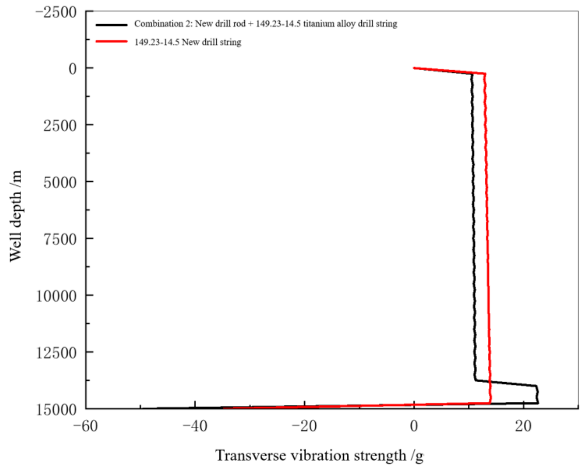

Figure 7. Transverse vibration strength of drill string.

3.2. Effect of Titanium Alloy Section Length on Composite Drill-String Dynamics

Figure 8 shows the whirling trajectories of composite drill strings with different titanium alloy section lengths at different well depths. The drill bit first swings irregularly at the bottom of the well and then changes to rolling motion along the wellbore wall. This behavior occurs because the rotational inertia of the drill string becomes increasingly important during drilling. The combined action of centrifugal force and wellbore-wall support causes the bit to roll along the wall. As well depth decreases, the whirling range of the drill string expands. In deep sections, the bottomhole weight on bit and formation support strongly constrain lateral displacement. At shallower depths, these constraints weaken, and the lateral freedom of the drill string increases, making the vibration energy transmitted from the bit more likely to generate a larger whirling motion. Near the wellhead, the rigid constraint of the wellhead equipment restricts lateral displacement; so, a large whirling motion is difficult to develop even when the vibration is transmitted upward. Compared with steel drill strings, titanium alloy drill strings have a lower elastic modulus and weaker resistance to lateral excitation. Under the same loading conditions, they therefore exhibit larger lateral deformation and a larger whirling range.

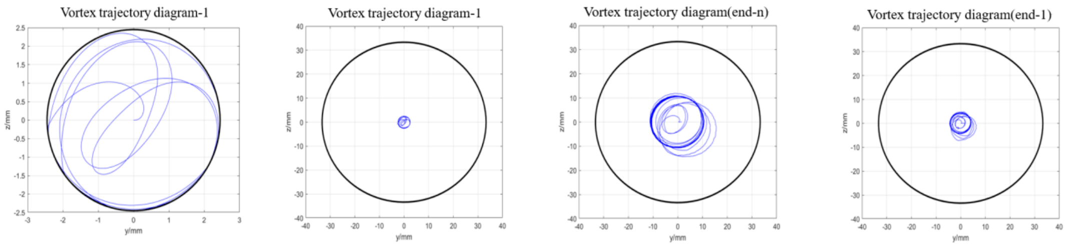

(**a**) Titanium alloy section length of 0 m

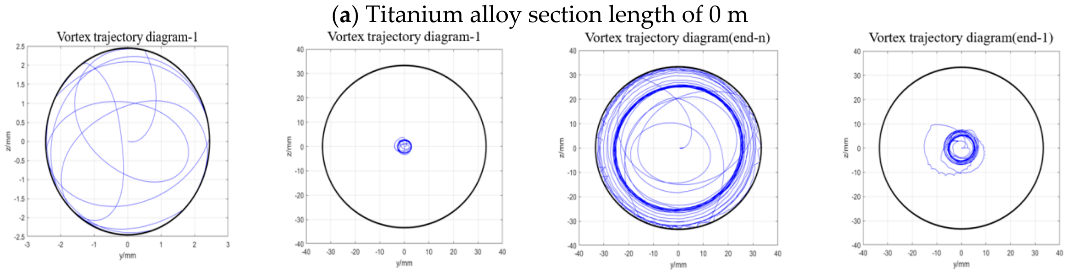

(**b**) Titanium alloy section length of 1000 m

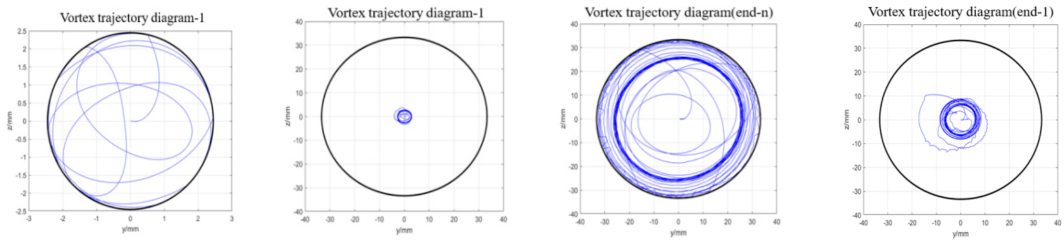

(**c**) Titanium alloy section length of 2000 m

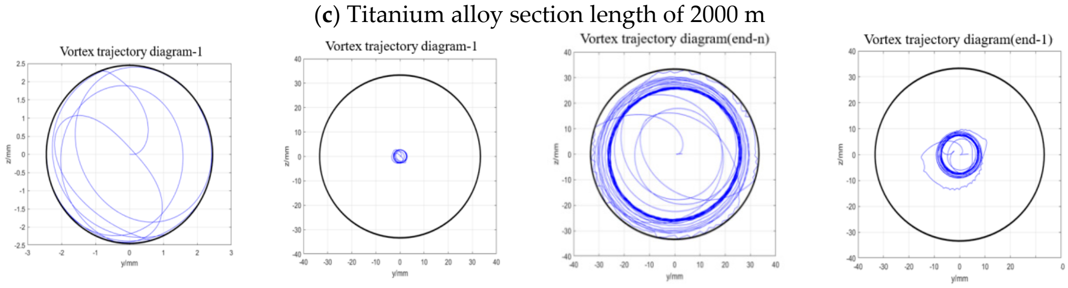

(**d**) Titanium alloy section length of 3000 m

Figure 8. Whirling trajectories corresponding to different titanium alloy lengths.

Figure 9 shows the lateral vibration intensity of drill strings with different titanium alloy section lengths as a function of well depth. Adding a titanium alloy section at the bottom reduces the lateral vibration intensity of the upper segment by approximately 30% compared with an all-steel drill string. Because the lower titanium alloy section has relatively low stiffness, it promotes the dissipation and dispersion of vibration energy during propagation. This attenuates vibration transmission to the upper drill string and reduces the lateral vibration intensity of the upper segment. As the length of the lower titanium alloy section increases, more vibration energy is absorbed and attenuated near the bottom, and less energy is transmitted upward. As a result, the overall lateral vibration intensity of the drill string gradually decreases.

Figure 10 shows the torsional vibration intensity of the composite drill string as a function of the well depth for different titanium alloy section lengths. Introducing a titanium alloy section near the bit or increasing its length reduces the overall torsional stiffness of the drill string. According to drill-string dynamics, lower torsional stiffness produces higher torsional deformation under the same applied torque, thereby increasing the torsional vibration intensity. As the length of the titanium alloy section increases, the torsional vibration intensity also increases, although the increase is gradual. This indicates a clear trade-off: a longer titanium alloy section is beneficial for attenuating the lateral vibration transmitted to the upper string, but it also weakens the torsional stiffness and may amplify the torsional response. Therefore, the installation length of the titanium alloy section should be selected carefully to satisfy the drilling requirements while avoiding an excessive reduction in torsional stiffness.

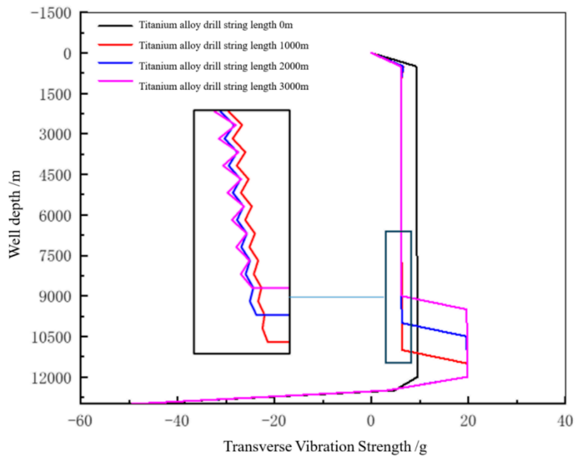

Figure 9. Transverse vibration strength of different titanium alloy drill string lengths.

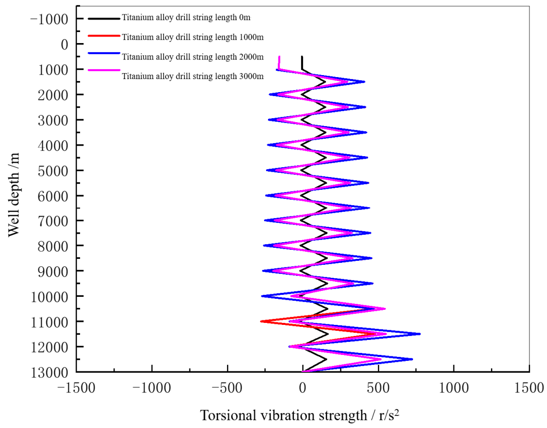

Figure 10. Torsional vibration strength of different titanium alloy drill string lengths.

3.3. Effect of Titanium Alloy Section Wall Thickness on Composite Drill-String Dynamics

Figure 11 shows the whirling trajectories of the upper drill string (Φ149.23 × 15.88 mm, U165) and the lower titanium alloy drill string (139.7 mm) under wall thicknesses of 9.17, 10.54, 12.7, and 15.88 mm. As the wall thickness of the titanium alloy drill string increases, the interaction between the drill bit and the wellbore wall changes from intermittent collision to continuous rolling friction. This sustained contact produces stable normal pressure and tangential friction on the bit tooth surface, which accelerates abrasive and adhesive wear. Increasing the wall thickness also increases the stiffness of the titanium alloy drill string and produces a more stable centrifugal-force distribution along the string. This suppresses the whirling amplitude, reduces the probability of contact with the wellbore, and lowers the wear risk in the middle drill-string section. When the wall thickness exceeds 12.7 mm, the drill string reaches a dynamically self-stabilizing state and can operate without contacting the wellbore wall. This condition can substantially improve the drill-string service life and safety. Therefore, drill-bit wear and overall drill-string safety can be balanced by properly controlling the wall thickness.

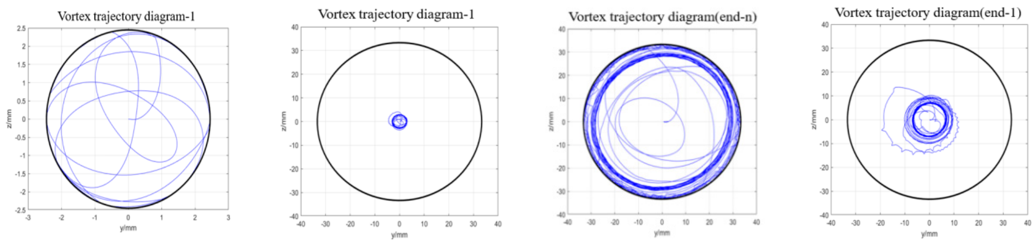

(**a**) Titanium alloy drill string wall thickness of 9.17 mm

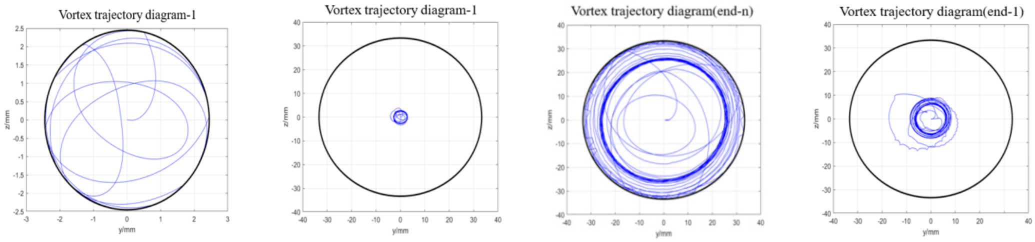

(**b**) Titanium alloy drill string wall thickness of 10.54 mm

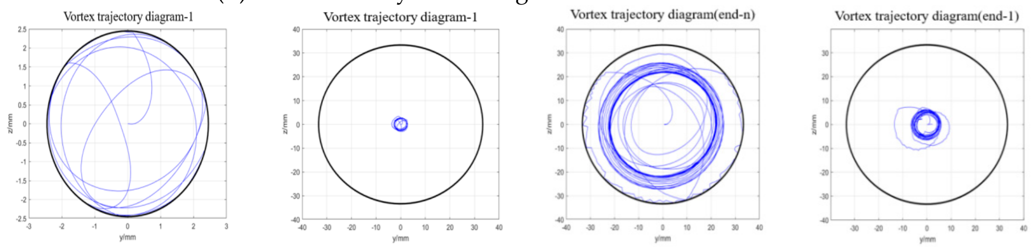

(**c**) Titanium alloy drill string wall thickness of 12.7 mm

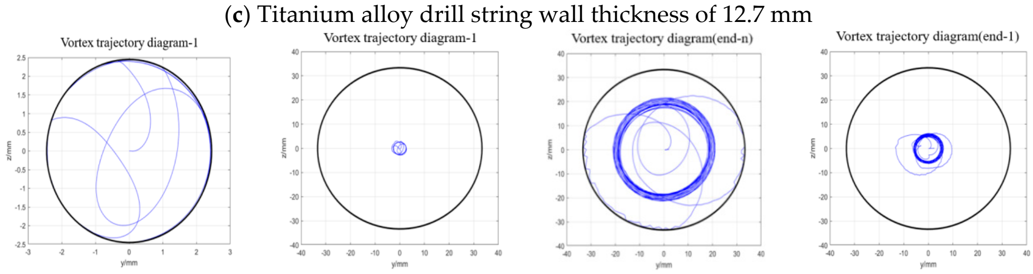

(**d**) Titanium alloy drill string wall thickness of 15.88 mm

Figure 11. Whirling trajectories corresponding to different titanium alloy drill string wall thicknesses.

Figure 12 shows the lateral vibration intensity of the composite drill string under different wall thicknesses. Increasing the wall thickness increases the stiffness and deformation resistance; so, the vibration amplitude of the titanium alloy section decreases under the same external excitation, and its lateral vibration intensity gradually declines. Because the steel and titanium alloy sections have markedly different stiffness, vibration-energy transmission across the material interface is weakened, reducing the ability of the titanium alloy section to transmit vibration energy to the adjacent upper steel section. The relatively small stiffness changes caused by varying the wall thickness of the titanium alloy section have only a limited influence on the vibration characteristics of the upper steel drill string. Therefore, changes in the wall thickness of the lower titanium alloy section have a limited effect on the lateral vibration intensity of the upper section.

Figure 13 shows the torsional vibration intensity for titanium alloy drill strings with different wall thicknesses. Increasing the wall thickness increases the drill-string rigidity and improves the resistance to deformation. As a result, the torsional vibration decreases progressively. Within the tested range, increasing the wall thickness of the titanium alloy section improves the bending and torsional rigidity and helps improve the drilling stability.

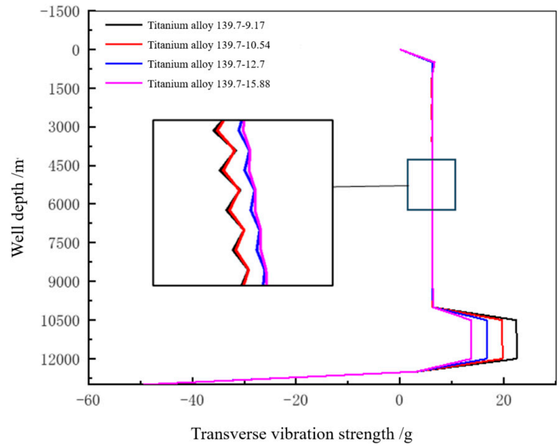

Figure 12. Transverse vibration strength of different titanium alloy drill string wall thicknesses.

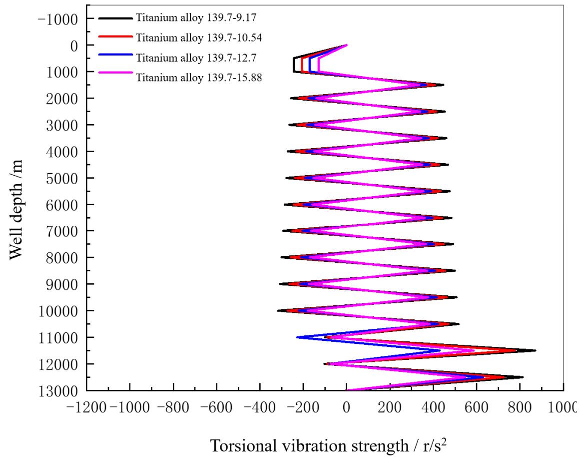

Figure 13. Torsional vibration strength of different titanium alloy drill string wall thicknesses.

3.4. Effect of Titanium Alloy Section Installation Position on Composite Drill-String Dynamics

Figure 14 shows the effect of different titanium alloy drill-string installation positions on the whirling trajectories at different well depths. Compared with installing the titanium alloy section near the bottom of the well, installing it in the middle changes the mass distribution of the lower drill string and helps the lower section maintain a more stable rotational state. This promotes more regular whirling and reduces random collisions between the drill bit and the wellbore wall. As a result, the bit motion changes from erratic impacts to more organized rolling contact, which reduces the risk of fatigue failure near the bit. A middle-position titanium alloy section also stabilizes the lower drill string and suppresses the expansion of the whirling range in the upper drill string caused by unstable lower-section motion. This arrangement reduces the probability of wellbore contact and lowers the risk of wear.

Figure 15 shows the lateral vibration of the titanium alloy drill string versus well depth for different installation positions. When the titanium alloy section is installed in the middle, its lower stiffness makes it the main region for vibration-energy dissipation. Bending deformation in this section absorbs part of the vibration energy through internal material damping. At the steel–titanium stiffness transition points, vibration waves are also reflected and scattered, reducing the energy propagation along the drill string. Compared with installation near the bit, middle installation interacts with the upper wellbore constraints to form a stable structure with a flexible buffer in the middle and rigid constraints at both ends. This configuration shifts the center of gravity toward the middle, improves the rotational dynamic stability, and reduces the overall lateral vibration intensity by approximately 30%.

It also reduces contact between the drill string and the wellbore, further lowering the risk of wear.

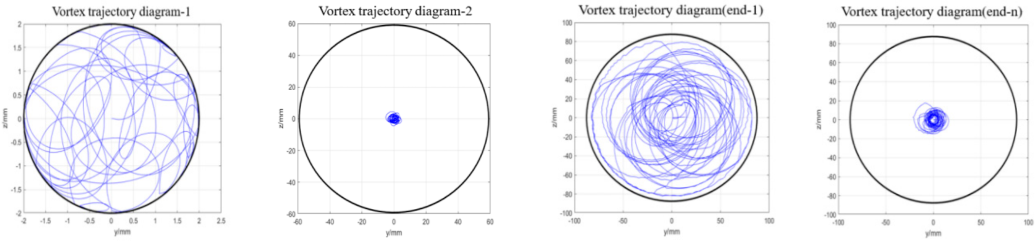

(**a**) Scheme 4

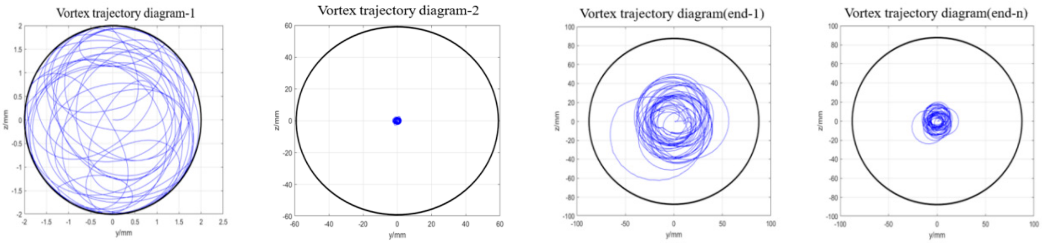

(**b**) Scheme 5

Figure 14. Whirling trajectory of drill bit, well depth 11,250 m, well depth 7500 m and well depth 250 m.

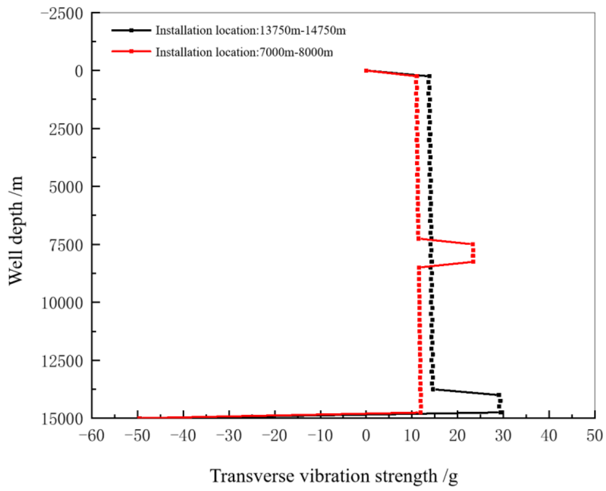

Figure 15. Transverse vibration strength.

Figure 16 shows the torsional vibration of titanium alloy drill strings with depth for different installation positions. Installing the titanium alloy section in the middle significantly reduces the torsional vibration intensity and improves the operational stability. In this position, the section acts as a central mass-distribution region, which promotes rotational stability and suppresses the torsional vibration amplification caused by uneven mass distribution. The middle section also serves as an energy-absorption region. When torsional vibration energy reaches the titanium alloy segment, elastic deformation in this segment absorbs part of the energy and reduces the energy transmission upward and downward. Consequently, the overall torsional vibration intensity of the drill string is reduced. Middle installation reduces the torsional vibration intensity by approximately 40% compared with installation near the bit.

https://doi.org/10.3390/app16189097

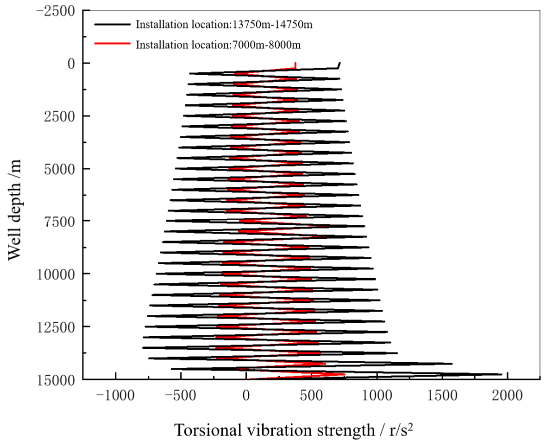

Figure 16. Torsional vibration strength.

4. Discussion

4.1. Comparison with Previous Studies and Model Applicability

The main trends obtained in this study are consistent with published studies on titanium/steel composite drill strings and nonlinear drill-string dynamics. Liu et al. [25] and Chen et al. [26] reported that titanium/steel composite configurations can change the dynamic stress and vibration distribution because of the stiffness and mass mismatch between material sections. The present results further quantify how the section length, wall thickness, and installation position modify whirling, lateral vibration, and torsional vibration. The observed importance of the torsional stiffness is also consistent with the coupled torsional–axial vibration and stick–slip studies of Kessai et al. [19,20].

A direct experimental or field validation for the exact 15,000 m composite drill-string configuration is not currently available. As a partial verification, the model uses established Euler–Bernoulli beam dynamics, Hertz contact, Rayleigh damping, and Newmark integration, and the predicted qualitative trends agree with previous validated numerical and experimental observations of drill-string vibration [11,25,26]. Therefore, the present results should be used primarily for comparative design and parameter screening. Quantitative field prediction will require calibration against downhole vibration measurements.

The contact and formation parameters also affect the vibration response. In this study, the formation stiffness, borehole–wall contact stiffness, friction coefficient, WOB, rotational speed, and boundary/support conditions are kept constant so that the influence of titanium alloy structural parameters can be isolated. If softer formations, higher friction coefficients, curved well trajectories, or different support conditions are encountered, the absolute vibration amplitudes and contact forces may change. However, the comparative trends are expected to remain useful, as long as the response is dominated by stiffness and mass redistribution in the drill string.

4.2. Design Implications of Titanium Alloy Section Parameters

The expression “appropriate increase in wall thickness” refers to the tested wall-thickness range in which increasing the titanium alloy wall thickness improves the bending and torsional rigidity without introducing unnecessary weight and cost. In the present simulations, 12.7 mm is treated as a recommended lower limit for stable operation, whereas larger values such as 15.88 mm may provide additional stiffness but must be evaluated against the manufacturing cost, material availability, connection design, and handling weight. The higher cost of titanium alloy and increased wall thickness may be offset when longer service life, lower wear, reduced failure risk, and improved operational safety are required.

The recommendation to install the titanium alloy section in the middle of the drill string is condition-dependent. It is supported by the simulated well depth, wellbore geometry, rotational speed, WOB, contact parameters, and composite string layout used in this work. For other well trajectories or operating conditions, the middle-position concept should be re-evaluated using the same modeling workflow before field implementation.

The parameter recommendations in this study are obtained from comparative sensitivity analysis rather than from a formal mathematical optimization algorithm. The evaluation criteria include (i) reducing the whirling range and wellbore-wall impact frequency, (ii) reducing the lateral vibration intensity of the upper drill string, (iii) avoiding excessive torsional vibration caused by reduced torsional stiffness, and (iv) maintaining sufficient wall thickness to improve the bending and torsional rigidity. Under these criteria, the tested schemes indicate that a titanium alloy section length of 1000–2000 m provides a practical compromise. A longer titanium alloy section further attenuates lateral vibration transmission, but it also lowers the torsional stiffness and increases the torsional vibration tendency.

4.3. Mechanism, Limitations, and Future Work

The vibration attenuation mechanism can be understood from the stiffness and mass mismatch between steel and titanium alloy sections. The titanium alloy section has a lower elastic modulus and density; so, it changes the impedance distribution of the drill string. At the steel–titanium transition, part of the vibration wave is reflected and scattered, while another part is dissipated through bending deformation and equivalent damping in the titanium alloy section. This impedance mismatch and wave-propagation effect reduces vibration transmission to the upper steel drill string, although it may increase the local vibration in the titanium alloy section.

Because the composite design changes the torsional stiffness distribution, it may also affect the stick–slip behavior. The present model includes the torsional vibration response and bit torque excitation but does not explicitly solve a full nonlinear stick–slip instability model with detailed bit–rock friction law and drilling-fluid coupling. Therefore, the influence of the recommended configuration on stick–slip onset, stick–slip amplitude, and fatigue life should be regarded as a limitation of the present work and will be investigated in future studies using coupled axial–torsional stick–slip models and field validation.

5. Conclusions

Increasing the drill-string diameter reduces the whirling range and wall-impact frequency. In the simulated schemes, when the diameter exceeds 149.23 mm, drill string-wall collisions decrease, which is beneficial for reducing vibration and wear.

Increasing the drill-string diameter also reduces the transverse vibration intensity. Compared with the steel section, the titanium alloy section shows approximately 60% higher local transverse vibration intensity, whereas the drill string above the titanium alloy section shows an approximately 18% reduction in transverse vibration. This indicates that titanium alloy sections should be selected with sufficient diameter and stiffness to balance local deformation and upper-string vibration attenuation.

Installing the titanium alloy section in the middle of the drill string reduces the overall lateral vibration intensity by approximately 30% compared with near-bit installation and reduces the torsional vibration intensity by approximately 40%. This configuration is recommended for conditions similar to those simulated in this study, because it provides a better balance between vibration attenuation and torsional stability.

Within the simulated parameter set, comparative sensitivity analysis supports the following recommended titanium alloy section parameters: an installation length of

1000–2000 m, a diameter of at least 139.7 mm, and a wall thickness of at least 12.7 mm. These values should be interpreted as design recommendations for the tested ultra-deep vertical-well conditions rather than universal optima.

The main limitation of this study is that direct field or laboratory validation for the exact 15,000 m steel–titanium alloy configuration is not yet available. Future work will focus on field-data calibration, high-resolution figure presentation, non-vertical well trajectories, fluid–structure interaction, nonlinear material behavior, and coupled axial–torsional stick–slip fatigue analysis.

Author Contributions: Conceptualization, J.W. and S.H.; Methodology, W.H., M.Y., A.F. and Q.D.; Software, X.H.; Validation, Y.W.; Formal analysis, H.L. and T.H.; Investigation, J.W., S.Y., X.H., H.L., Y.W., A.F. and Q.D.; Resources, X.H., W.H., M.Y. and Q.D.; Data curation, W.H., S.H., M.Y., Y.W., A.F. and T.H.; Writing—original draft, S.Y. and T.H.; Writing—review & editing, J.W., X.H. and H.L.; Visualization, S.Y., H.L. and W.H.; Supervision, X.H., H.L., Y.W. and T.H.; Project administration, X.H., W.H., A.F., T.H. and Q.D.; Funding acquisition, X.H., S.H., M.Y., A.F. and Q.D. All authors have read and agreed to the published version of the manuscript.

Funding: This research is supported by the National Natural Science Foundation of China (52274004) Research on Driving Mechanism and Automatic Control of Electricdrill for Coiled Tubing Intelligent Drilling, the Chongqing Natural Science Foundation Joint Fund for Innovation and Development (CSTB2023NSCQ-LZX0132), the National Key Research and Development Program of China (No. 2023YFC3009200), Key Science and Technology Projects for Basic and Prospective Research of CNPC (No. 2023ZZ11 and No. 2025DJ106), MIIT Fundamental public service platform for industrial technology (TC230A077).

Institutional Review Board Statement: Not applicable.

Informed Consent Statement: Not applicable.

Data Availability Statement: The original contributions presented in this study are included in the article. Further inquiries can be directed to the corresponding authors.

Acknowledgments: During the preparation of this manuscript, the authors used Doc2X V3-2026 to translate the manuscript from Chinese into English and DeepSeek V4 for partial language editing. The authors reviewed and edited the output and take full responsibility for the content of this publication.

Conflicts of Interest: The authors declare no conflicts of interest.

References

1. Dong, G.; Chen, P. A review of the evaluation, control, and application technologies for drill string vibrations and shocks in oil and gas well. *Shock Vib.* **2016**, *2016*, 7418635. [CrossRef]
2. Afriansyah, A.; Basri, H. A Review Dynamic Vibration on Drill String in Drilling Operation. *Sebatik* **2019**, *23*, 1–8. [CrossRef]
3. Fu, M. Research on the Nonlinear Vibration Mechanism and Control Method of Drilling Column System. Doctoral Dissertation, Northwestern Polytechnical University, Xi'an, China, 2019.
4. Khulief, Y.A.; Al-Sulaiman, F.A.; Bashmal, S. Vibration analysis of drillstrings with self-excited stick–slip oscillations. *J. Sound. Vib.* **2007**, *299*, 540–558. [CrossRef]
5. Christoforou, A.P.; Yigit, A.S. Dynamic modelling of rotating drillstrings with borehole interactions. *J. Sound. Vib.* **1997**, *206*, 243–260. [CrossRef]
6. Naganawa, S.; Sato, R.; Ishikawa, M. Cuttings-transport simulation combined with large-scale-flow-loop experimental results and logging-while-drilling data for hole-cleaning evaluation in directional drilling. *SPE Drill. Complet.* **2017**, *32*, 194–207. [CrossRef]
7. Di, Q.; Wang, W.; Yao, Y.; Zhu, W.; Yao, J.; Hu, Y. Dynamic Model and Whirling Motion Characteristics Simulation of Bottom-Hole Assembly Tools. *J. China Univ. Pet. (Nat. Sci. Ed.)* **2010**, *34*, 53–56.
8. Di, Q.; Yang, H.; Wang, W.; Luo, D.; Zhang, H.; Chen, F. Research Progress and Development Trends of Borehole Dynamics. *Pet. Sci. Bull.* **2024**, *9*, 224–239.
9. Wang, W.; Hu, Q.; Liu, H.; Zhang, W. Vertical Vibration Analysis and Application of Drilling Rod. *Vib. Impact* **2011**, *30*, 229–233.
10. Teng, X.; Di, Q.; Li, N.; Chen, F.; Zhou, B.; Wang, M. Measurement and Analysis of Vibration Characteristics of Ultra-Deep Well Drillstring Stick-Slip. *Pet. Drill. Technol.* **2017**, *45*, 32–39.

11. Al Shekaili, A.; Afebu, K.O.; Liu, Y.; Papatheou, E. Experimental analysis of drillstring vibrations using a small-scale drilling rig. *Nonlinear Dyn.* **2025**, *113*, 17491–17518. [CrossRef]
12. Li, X.; Li, X.; Li, K.; Zhang, H.; Chen, T. Experimental Research on Axial-Torsional Coupling Vibration of Drilling Rod. *J. Vib. Impact* **2024**, *43*, 314–320.
13. Mao, L.; Zhao, X.; Zhang, L.; He, X.; Zhu, F. Analysis of Stick–Slip Vibration Characteristics of an Axial–Torsional Coupled Vibration Model in Horizontal Drill Strings. *Arab. J. Sci. Eng.* **2025**, *51*, 15319–15338. [CrossRef]
14. Wang, B.; Ren, F.; Zhu, A.; Zhao, L. Numerical Analysis and Experimental Study on Whirling Characteristics of Horizontal Well Drill Strings. *Chin. J. Mech. Eng.* **2018**, *29*, 696–704.
15. Cao, Y.; Li, H.; Wan, Z.; Dou, Y. Analysis of Casing Wear Degree Induced by Whirling Drill String in Well Repair Drilling. *Pet. Mach.* **2021**, *49*, 125–132.
16. Tikhonov, V.S.; Safronov, A.I. Numerical simulation of the drillstring-in-hole dynamics at rotary drilling. *Eng. Syst. Des. Anal.* **2008**, *48364*, 543–550. [CrossRef]
17. Liu, J.; Zhang, B.; Wang, F. Research on Dynamic Characteristics of Deep and Extra-Deep Well Drill Strings Based on Finite Element Simulation. *China Pet. Chem. Stand. Qual.* **2025**, *45*, 150–152.
18. Di, Q.; You, M.; Li, T.; Zhou, X.; Yang, H.; Wang, W. Simulation and Analysis of Ultra-Deep Well Drillstring Dynamic Characteristics. *Pet. Drill. Technol.* **2024**, *52*, 108–117.
19. Kessai, I.; Benammar, S.; Doghmane, M.Z. Dynamic failure analysis and lifetime estimation of tool-string in rotary drilling system under torsional-axial coupled vibrations. *Eng. Fail. Anal.* **2022**, *134*, 106037. [CrossRef]
20. Kessai, I.; Benammar, S.; Doghmane, M.Z.; Tee, K.F. Drill bit deformations in rotary drilling systems under large-amplitude stick-slip vibrations. *Appl. Sci.* **2020**, *10*, 6523. [CrossRef]
21. Phuor, T.; Yoon, G.H. Eigensensitivity of damped system with distinct and repeated eigenvalues by chain rule. *Int. J. Numer. Methods Eng.* **2023**, *124*, 4687–4717. [CrossRef]
22. Phuor, T.; Yoon, G.H. Model order reduction for Campbell diagram analysis of shaft-disc-blade system in 3D finite elements. *Struct. Eng. Mech.* **2022**, *81*, 411–428.
23. United Nations. *Transforming Our World: The 2030 Agenda for Sustainable Development*; United Nations: New York, NY, USA, 2015.
24. Cheng, J. Research on the Overall Whirling and Joint Ultimate Load-Carrying Capacity of Deep and Extra-Deep Well Aluminum Alloy Drill Pipe. Doctoral Dissertation, Jilin University, Changchun, China, 2022.
25. Liu, Q.; Zhou, B.; Chen, F.; Li, N.; Xie, J.; Zhao, M.; Di, Q.; Feng, C.; Song, S.; Yin, C. Optimal design and nonlinear dynamic characteristics of titanium/steel drill pipe composite drill string for ultra-deep drilling. *Sci. Rep.* **2023**, *13*, 20491. [CrossRef] [PubMed]
26. Chen, F.; Bin, G.; Liu, Z.; Zhang, J.; Guo, W.; Wu, Y.; Wang, W.; Liu, Q.; Di, Q. Dynamic Characteristic Analysis and Optimal Design of Titanium Alloy/Steel Drill Pipe Composite Drillstring. *J. China Univ. Pet. (Nat. Sci. Ed.)* **2024**, *48*, 75–83.
27. Johnson, K.L. One hundred years of Hertz contact. *Proc. Inst. Mech. Eng.* **1982**, *196*, 363–378. [CrossRef]

https://doi.org/10.3390/app16189097